Omega-k Algorithm Implementation for Linear Frequency Modulated-Continous Wave SAR Signal Processing

Jhohan Jancco Chara
Escuela Profesional de Ingeniería Electrónica
Universidad Nacional de San Antonio Abad del Cusco
Cusco, Peru
111875@unsaac.edu.pe

Facundo Palomino Quispe
Escuela Profesional de Ingeniería Electrónica
Universidad Nacional de San Antonio Abad del Cusco
Cusco, Peru
facundo.palomino@unsaac.edu.pe

Roger Jesus Coaquira Castillo
Escuela Profesional de Ingeniería Electrónica
Universidad Nacional de San Antonio Abad del Cusco
Cusco, Peru
roger.coaquira@unsaac.edu.pe

Mark Clemente-Arenas
Grupo de Circuitos y Sistemas Electronicos de Alta Frecuencia ECS-HF
Universidad Nacional Tecnológica de Lima Sur UNTELS
Lima, Peru
mclemente@untels.edu.pe.

***Abstract*—The Omega-k algorithm is used for SAR systems due to the precision on focus quality in SAR raw signal. However, it is little explored for specific SAR systems such as Linear Frequency Modulated Continuous Wave LFM-CW systems. These systems are used to distance to target estimation, mapping, 3D modelling, etc. In this paper, the Omega-k algorithm is implemented for LFM-CW radars focusing real and simulated SAR raw signal determining algorithm focus quality parameters.**

Keywords— Synthetic Aperture Radar SAR, Linear frequency modulated continuous wave LFM-CW, Omega-k algorithm.

I. INTRODUCTION

In recent decades, synthetic aperture radar SAR has become a primary instrument for remote observation of the Earth due to the ability to penetrate the Earth's surface. A SAR with continuous wave frequency linear modulation is used due to its low cost in hardware implementation. This is an important advantage over pulsed SAR sensors, whose advantage is precision. Synthetic aperture radars have applications in various fields such as agriculture, forest cover, topography, military surveillance, monitoring of earthquakes and the environment [1]. In the other hand, there are various effective processing algorithms for systems SAR pressed used mainly on space platforms, the most used are: range Doppler rD algorithm[2], Chirp-Scaling algorithm[3] and Omega-k algorithm [4]. The last one, has better performance in focusing of SAR raw signal, therefore, we developed Omega-k algorithm for LFM-CW SAR sensors generally installed on board an aerial platform based on the theory of the algorithm Omega-k precise version [3] and compare it with the range Doppler rD algorithm that is more used in this context.

This paper is organized in three sections. After this introductory section, the second section presents SAR signal modelling. Section three shows signal processing through Omega-K algorithm. Section four deals with results presentations and discussions at the end.

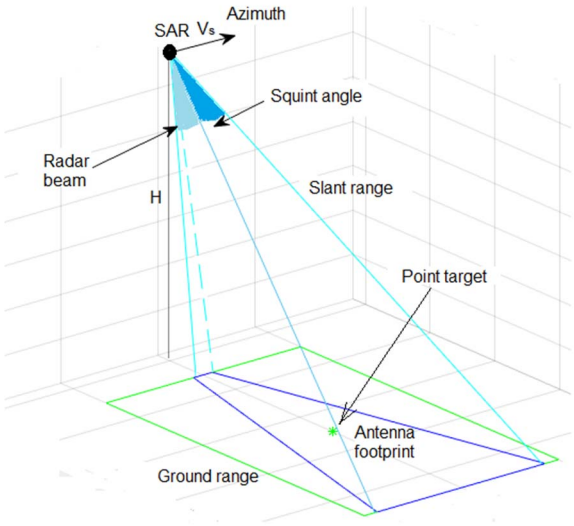

Fig. 1. Geometry of SAR Systems

II. SIGNAL MODELLING

A. Synthetic Aperture Radar

A LFM-CW SAR radar is an active sensor installed on board an aerial platform that has linear displacement with a constant speed. Whose antennas transmit a continuous wave signal modulated in linear frequency. Waves propagate to the desired surface in the direction perpendicular to the direction of movement called azimuth as seen in Fig. 1.

B. LFM-CW Chirp Signal

The signal in the transmission is s_t, therefore the signal in the reception s_r described by (1) and (2):

$$s_t(t) = exp\left(j(2\pi f_0 t + \pi k_r t^2)\right) \quad (1)$$

$$s_r(t) = exp\left(j(2\pi f_0 (t - \Delta t) + \pi k_r (t - \Delta t)^2)\right) \quad (2)$$

Where: f_0 is the chirp signal center frequency. t_p is the pulse duration. k_r is the chirp signal modulation rate and Δt is time delay.

978-1-7281-9377-9/20/$31.00 ©2020 IEEE

The signal $s_r(t)$ is displaced by a delay time $\Delta t = \frac{2\alpha R}{c}$, being $\alpha = \frac{c^2}{c^2 - v^2}$ Doppler factor [6], [7] and R is the distance between the sensor and point target [5] expressed as a function of time in azimuth *n* and the speed of the SAR sensor V_s in (3).

$$R(n) = \sqrt{{R_o}^2 + (V_s n)^2} \tag{3}$$

The backscatter signal $s_r(t)$ is captured by the receiving antennas of the SAR sensor, then these generally go through the steps including: mixer, bandpass filter, the mixer and the low pass filter. The resulting signal is defined by (4).

$$s_{dc}(t) = s_t(t) * s_r(t)$$

$$s_{dc}(t,n) = exp\left(j(2\pi f_0 \Delta t + 2\pi k_r t \Delta t - \pi k_r \Delta t^2)\right) \tag{4}$$

Signal s_{dc}[8]is useful for simulating raw SAR data in the time domain, which is useful for testing the focus algorithms.

C. Two Dimensional Domain

The Omega-k algorithm is used to perform signal processing in the two-dimensional frequency domain. Therefore, signal s_{dc} is expressed in two-dimensional frequency domain.

In the SAR raw signal s_{dc}, the term $\Delta t^2 \to 0$ so the expression $\pi k_r \Delta t^2$ is neglected for SAR signal processing therefore, the raw signal expressed by (5).

$$s_o(t,n) = exp\left(j(2\pi f_0 \Delta t + 2\pi k_r t \Delta t)\right) \tag{5}$$

SAR signal processing is implemented considering only the signal phase. Then, the Fourier transform in range is first calculated as seen in (6), and the central frequency f_o is intervened by the frequency in range: $f_o \to f_o + f_t$,[5].

$$S(f_t, n) = \int_{\frac{-t_o}{2}}^{\frac{t_o}{2}} s_o(t, n) \exp(-j2\pi f_t t)\, dt$$

$$S(f_t,n) = t_o sinc(\pi t_o(f_t - k_r \Delta t)) exp(2\pi(f_o + f_t)\Delta t) \tag{6}$$

Then we calculate the Fourier transform in azimuth.

$$S(f_t, f_n) = \int_{-\infty}^{\infty} s_o(f_t, n) \exp(-j2\pi f_n n)\, dn$$

Whose phase is $\theta(n)$ expressed in time domain in azimuth. This phase is maximized by a derivative with respect to the time domain, and taking into account[3], we proceed to solve as seen in (7).

$$\theta(n) = \frac{4\pi\alpha(f_o + f_t)}{c} \sqrt{{R_o}^2 + (V_s n)^2} - j2\pi f_n n \tag{7}$$

$$\frac{d\theta(n)}{dn} = 0$$

Then, we obtain (8):

$$n = \frac{c f_n R_o}{2\alpha V_s \sqrt{(f_o + f_t)^2 - \left(\frac{c f_n}{2\alpha V_s}\right)^2}} \tag{8}$$

Replacing equation (8) in (7), we obtain:

$$\theta(f_t, f_n) = \frac{4\pi\alpha R_o}{c} \sqrt{(f_o + f_t)^2 - \left(\frac{c f_n}{2\alpha V_s}\right)^2}$$

Finally, the SAR raw signal in the two-dimensional domain is expressed by (9):

$$S(f_t, f_n) = t_o sinc\left(\pi t_o (f_t - k_r \Delta t)\right) exp\left(j\theta(f_t, f_n)\right) \tag{9}$$

Where: $\theta(f_t, f_n) = \frac{4\pi\alpha R_o}{c} \sqrt{(f_o + f_t)^2 - \left(\frac{c f_n}{2\alpha V_s}\right)^2}$

III. Signal Processing

A. OMEGA-K Algorithm

The implementation of the Omega-k algorithm for SAR systems LFM-CW is based on the precise version that is used in pulsed SAR systems. The general description of the algorithm for SAR LFM-CW systems is shown in the following block diagram.

Fig. 3. shows that the two-dimensional Fourier transform is applied to the SAR raw signal. Then, the raw signal in the two-dimensional domain is multiplied by a reference function known as this step as bulk focusing. The phase of the reference function is described by (10):

$$\theta_{ref}(f_t, f_n) = -\frac{4\pi\alpha R_{ref}}{c} \sqrt{(f_o + f_t)^2 - \left(\frac{c f_n}{2\alpha V_s}\right)^2} \tag{10}$$

Then, the reference function is multiplied with the raw signal in the two-dimensional domain obtaining (11):

$$\theta_{RFM}(f_t, f_n) = \frac{4\pi\alpha(R_o - R_{ref})}{c} D(f_t, f_n) \tag{11}$$

Where: $D(f_t, f_n)$ is the quadratic factor in the two-dimensional frequency domain.

$$D(f_t, f_n) = \sqrt{(f_o + f_t)^2 - \left(\frac{c f_n}{2\alpha V_s}\right)^2}$$

Differential focusing also called stolt interpolation is implemented by replacing variables from f_t to f_t' as seen in (12). Similar to the case of pulsed SAR radar[4]. The variable f_t' is implemented using a difference between the quadratic factor in the two-dimensional domain and the quadratic factor in the range Doppler domain [5] to solve the range cell migration curve.

$$f_t' = D(f_t, f_n) - D(f_n)$$

$$f_t' = \sqrt{(f_o + f_t)^2 - \left(\frac{c f_n}{2\alpha V_s}\right)^2} - f_o \sqrt{1 - \left(\frac{c f_n}{2\alpha V_s f_o}\right)^2} \tag{12}$$

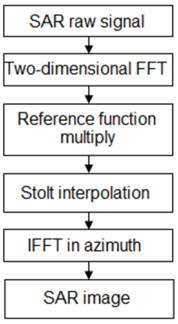

Fig. 2. Modified Omega-k algorithm

B. *Impulse Response*

The impulse response is obtained by focusing the SAR raw signal from an isolated isotropic point target as seen in Fig. 3.

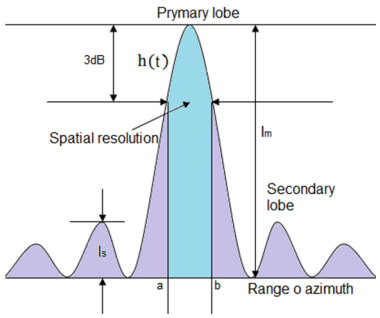

Fig. 3. Impulse response function.

Where: h(t) is the Impulse response function. a y b are the half power points or 3dB. I_s is the maximum intensity of the secondary lobe and I_m is the maximum intensity of the primary lobe.

Then, the impulse response function allows determining the quality parameters of which are: spatial resolution, ISLR and PSLR.

The spatial resolution is defined with range and azimuth resolutions as in (13).

$$\delta_R = \frac{c}{2B} \; y \; \delta_A = \frac{\lambda_0}{2\Delta\theta} \tag{13}$$

Where: δ_R is the range resolution. δ_A is the Azimut resolution. C is the speed of light. B is the Bandwidth. λ_0 is the wavelength. $\Delta\theta$ is the Squint angle.

The ISLR and PSLR parameters are calculated with (14) and (15):

$$PSLR = 10log\left(\frac{I_s}{I_m}\right) \tag{14}$$

$$ISLR = 10log\left(\frac{\int_{-\infty}^{a}|h(t)|^2dt+\int_{b}^{\infty}|h(t)|^2dt}{\int_{a}^{b}|h(t)|^2dt}\right) \tag{15}$$

IV. RESULTS

A. *Impulse Response*

SAR raw signal of a point target is simulated to determine the quality parameters of the Omega-k algorithm, taking into account the initial parameters of Table I.

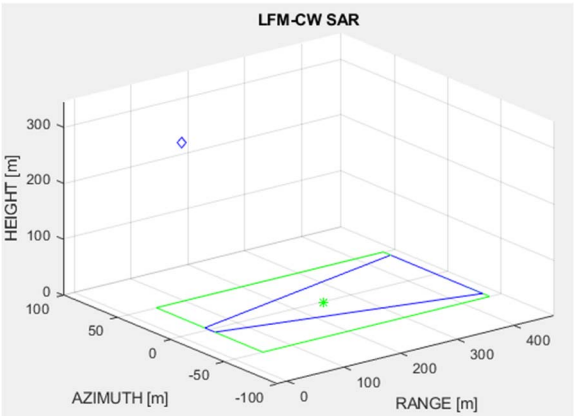

Fig. 4. SAR LFM-CW simulation.

TABLE I. INITIAL PARAMETERS

SAR LFM-CW Parameters	
Symbol	***Value***
f_0	5.42876GHz
B	170 MHz
f_s	24.875MHz
PRF	307.292Hz
$\Delta\theta$	11°
V_s	30.1938 m/s
c	$3*10^8$ m/s

Where: f_s is the sampling rate and PRF Pulse repetition frequency.

Then, the SAR raw signal obtained by simulation generated a SAR image of an isolated and isotropic point target shown in the Fig. 5.

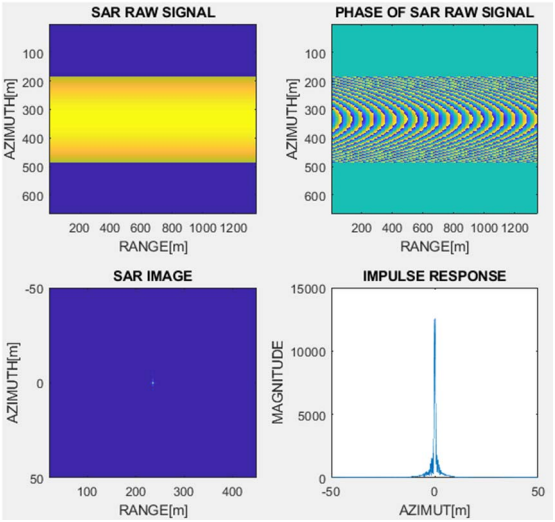

Fig. 5. Impulse response.

The resolution in range and azimuth is determined using equation 13, whose values are: $\delta_R = 0.88$ m and $\delta_A = 0.144$m.

The quality parameters obtained experimentally using the impulse response and equations 14 and 15. The following results were obtained, shown in Table II.

TABLE II. QUALITY PARAMETERS IN RANGE AND AZIMUTH

Symbol	***Value***
δ_R	0.9m
$PSLR_R$	-8.56dB
$ISLR_R$	-5.22dB
δ_A	0.14m
$PSLR_A$	-8.06dB
$ISLR_A$	-2.83dB
δ_R	0.9m

The quality parameters calculated in Table II are acceptable for the SAR LFM-CW raw data focusing. Furthermore, the omega-k algorithm was validated using the raw SAR data obtained by simulation.

B. *Validation with real raw signal*

MicroASAR [9] data courtesy of David G. Long at Brigham Young University [10], are the real SAR raw data acquired by sensor SAR LFM-CW aboard of an unmanned aerial vehicle whose photographic image of the sampled scene is shown is shown in Fig. 6.

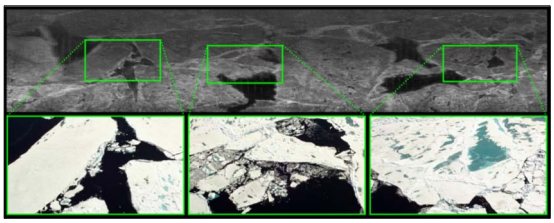

Fig. 6. MicroASAR and optical image [11].

The CASIE-09 microASAR sample data is provided in a file called flight9_9_sample.mat that contains two matrices such as: dat and geom. The geom matrix contains geometric data such as: time, latitude, longitude and altitude [12].

On the other hand, the dat matrix represents the raw SAR data of 3884 rows and 1702 columns, acquired with the radar parameters of Table 3. The SAR image generated by the Omega-k algorithm can be enhanced by an approximate range compensation described by the function t^3 [12]in the real SAR raw data focus.

TABLE III. MICROASAR PARAMETERS

MicroASAR Parameters	
Symbol	***Value***
f_0	5.42876GHz
B	170MHz
f_s	24.875MHz
PRF	307.292Hz
$\Delta\theta$	11^O
V_s	30.1938 m/s
c	$3*10^8$ m/s
k_r	$1.5972563681*10^{12}$
M	3884
N	1702

Where: M is the row of the SAR raw signal matrix and N is the column of the SAR raw signal matrix.

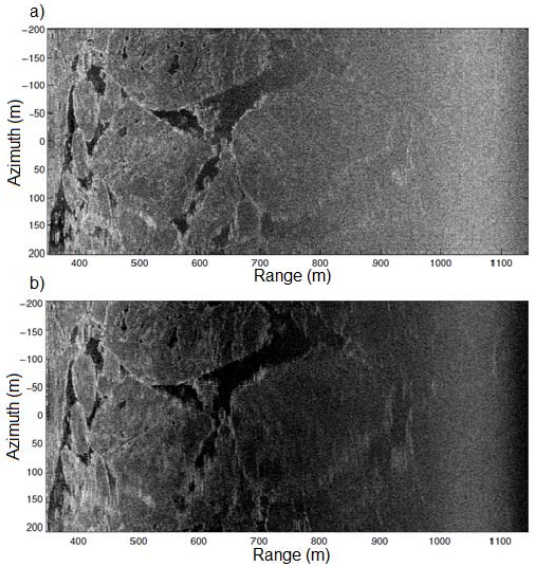

Fig. 7. Magnitude of the single look azimuth-compressed complex image from microASAR . a) Resulting image after using rD algorithm from [11], [12]. b) Resulting image after using Omega-K algorithm presented in this work.

In Fig. 7 is possible to notice that both rD algorithm (a) and Omega-K (b) were used were used to process raw data from [12]. As previously said rD is widely used in SAR signal processing, then it has been used as reference for validating our algorithm. Precise version of Omega-K algorithm works better to focus SAR data for high synthetic apertures compared to rD. Therefore, it was implemented for continuous wave radar to verify with SAR raw data CASIE-09 the with a squint width of 11 degrees. When we compare Fig. 7b) compared to Fig. 7a) obtained with the rG algorithm, a higher contrast was obtained. Some areas of the picture were better identified. The rG picture also shows more saturation in some regions which is indicative of noise.

V. CONCLUSION

The Omega-k algorithm for continuous wave synthetic aperture radars with linear frequency modulation was implemented in Matlab, which was validated with simulated SAR data and with real SAR raw data. On the other hand, the quality parameters of the Omega-k algorithm were determined using impulse response. The resolutions are 0.9m in range and 0.14m in azimuth. Processing using the Omega-k algorithm for continuous wave radars versus pulsed radars differs in stolt interpolation and inverse Fourier transform in azimuth, since for pulse radars the Fourier transform is performed in azimuth and range. Finally, the Omega-k algorithm can be improved, as a next step, by agreeing on motion compensation and filters to have a good quality image.

REFERENCES

[1] A. Zozaya, "Electromagnetic interaction models for the characterization of targets in SAR scenes: preliminary literature review," Ingeniería UC, vol. 22, no. 1, pp. 26-63, 2015.

[2] R. T. Lord and M. R. Inggs, "Efficient RFI suppression in SAR using LMS adaptive filter integrated with range/Doppler algorithm," *in Electronics Letters,* vol. 35, no. 8, pp. 629-630, 1999.

[3] R. K. Raney, H. Runge, R. Bamler, I. G. Cumming and F. H. Wong, "Precision SAR processing using chirp scaling," in IEEE Transactions on Geoscience and Remote Sensing, vol. 32, no. 4, pp. 786-799, July 1994.

[4] I. G. Cumming, Y. L. Neo and F. H. Wong, "Interpretations of the Omega-K Algorithm and Comparisons with other Algorithms," IGARSS 2003. 2003 IEEE International Geoscience and Remote Sensing Symposium (IEEE Cat. No.03CH37477), vol. 3, pp. 1455-1458, 2003.

[5] I. G. Cumming and F. H. Wong, Digital Processing of Synthetic Aperture Radar Data: algorithms and implementation, Norwood: Artech House, 2005.

[6] H. Bi, J. Wang and G. Bi, "Wavenumber Domain Algorithm-Based FMCW SAR Sparse Imaging," *IEEE Transactions on Geoscience and Remote Sensing,* vol. 57, no. 10, pp. 7466-7475, October 2019.

[7] R. Wang, O. Loffeld, H. Niels, S. Knedlik, M. Hagelen and H. Essen, "Focus FMCW SAR data using the wavenumber domain algorithm," IEEE Transactions on Geoscience and Remote Sensing, vol. 48, no. 4, pp. 2109-2118, 2010.

[8] E. C. Zaugg, "Generalized Image Formation for Pulsed and LFM-CW Synthetic Aperture Radar," 2010.

[9] M. Edwards, D. Madsen, C. Stringham, A. Margulis, B. Wicks and D. G. Long, "microASAR: A small, robust LFM-CW SAR for operation on UAVs and small aircraft." IGARSS 2008-2008 IEEE International Geoscience and Remote Sensing Symposium. Vol. 5. IEEE, 2008.

[10] C. Stringham and D. G. Long, "Improved processing of the CASIE SAR data," *2011 IEEE International Geoscience and Remote Sensing Symposium,* pp. 1389-1392, July 2011.

[11] E. Zaugg, D. Long, M. Edwards, M. Fladeland, R. Kolyer, I. Crocker, J. Maslanik, U. Herzfeld and B. Wallin,"Using the microASAR on the NASA SIERRA UAS in the characterization of Arctic sea ice experiment." *2010 IEEE Radar Conference*. IEEE, 2010.

[12] D. G. Long and C. Stringham. "The Sample BYU CASIE-09 MicroASAR Dataset." *Brigham Young University, Tech. Rep., October* 2011.